Digital light processing additive manufacturing of in situ mullite-zirconia composites

DE CAMARGO, Italo Leite, ERBERELI, Rogério, LOVO, João Fiore Parreira, FORTULAN, Raphael and FORTULAN, Carlos Alberto

This is a preprint of the follow the article published at Journal of the European Ceramic Society, Volume 42, Issue 13 , October 2022, Pages 6025-6032: The final authenticated version is available online at: https://doi.org/10.1016/j.jeurceramsoc.2022.06.042

Digital light processing additive manufacturing of in situ mullite-zirconia composites

Italo Leite de Camargo[1,2*], Rogério Erbereli[1], João Fiore Parreira Lovo[1], Raphael Fortulan[3], Carlos Alberto Fortulan[1]

[1]Department of Mechanical Engineering, São Carlos School of Engineering, University of São Paulo. Trabalhador São-carlense, 400, São Carlos, 13566-590, Brazil.

[2]Federal Institute of Education, Science and Technology of São Paulo - IFSP. Primeiro de Maio, 500. Itaquaquecetuba, SP, Brazil.

[3]Materials and Engineering Research Institute, Sheffield Hallam University, Sheffield S1 1WB, UK

Corresponding author: *italo.camargo@usp.br; +55 16 33739434

Abstract

Digital light processing (DLP) can produce small series ceramic parts with complex geometries and tiny structures without the high cost of molds usually associated with traditional ceramic processing. However, the availability of feedstock of different ceramics for the technique is still limited. Mullite-zirconia composites are refractory materials with diverse applications, nevertheless, their 3D printing has never been reported. In this work, alumina and zircon were used as raw materials for additive manufacturing by DLP followed by in situ mullite and zirconia formation. Thus, coarse zircon powder was milled to submicrometric size, alumina-zircon photosensitive slurries were prepared and characterized, parts were manufactured in a commercial DLP 3D printer, debound, and sintered at different temperatures. The printed parts sintered at 1600 ºC completed the reaction sintering and reached a flexural strength of 84 ± 13 MPa. The process proved capable of producing detailed parts that would be unfeasible by other manufacturing methods.

Keywords: 3D printing; Additive manufacturing; Digital light processing; Mullite; Zircon.

1 Introduction

Mullite-zirconia composites are important refractory materials with desirable fracture toughness and strength [1], being suitable for high-temperature applications as power generation engines, combustors, and in the glass melting and steel industry [1,2]. Reaction sintering is widely used to obtain mullite-zirconia composites. Such a route is easily scaled up industrially with conventional ceramic equipment [3,4] and it has the advantage of being able to use readily available materials as natural minerals as raw materials [1,3]. Alumina and zircon ($ZrSiO_4$) are extensively used as initial powders for being inexpensive raw materials [4]. The molar ratio 3:2 (alumina:zircon) is commonly used [1,5–8] for being the stoichiometric proportion for the formation of zirconia and mullite, as described in the following equation [6,9–11]. This reaction starts above 1400 ºC [12] and 1600 ºC may be required to complete it [1,6].

$$2ZrSiO_4 + 3Al_2O_3 - 3Al_2O_3.SiO_2 + 2ZrO_2 \quad (1)$$

Several forming methods (extrusion [13], pressing [3,14], slip casting [15,16], and gel casting [8]) have been studied in the manufacture of mullite-zirconia parts. However, the fabrication of such material by additive manufacturing (AM) has still been little explored and, to the best of our knowledge, has never been reported. AM allows the manufacturing of small series complex parts without the high cost of molds which are usually associated with traditional ceramic processing [17–19]. One of the main limitations for the widespread of ceramic AM is the shortage of suitable feedstock [20,21].

Digital Light Processing (DLP) is the ceramic AM technology that presents superior printing resolution, being able to produce tiny structures [22,23]. For that, proper photosensitive ceramic suspensions are required with at least 40 vol% of ceramic loading for avoiding defects in the heat treatment (debinding and sintering) [19,24]. On the other hand, the suspension must have controlled viscosity (<3 Pa.s) [17,19,24,25], to ensure the fluidity necessary for the formation of micrometric layers. Thus, the organic components (monomer, dispersant, photoinitiator, etc) must be carefully chosen and the ceramic powder must have the proper characteristics, such as suitable particle size.

In this work, mullite-zirconia parts were 3D printed for the first time. Thereunto, coarse zircon powder was processed, alumina-zircon photosensitive slurries were prepared and characterized, parts were manufactured in a commercial DLP 3D printer,

debound, and sintered at different temperatures to evaluate the in situ mullite and zirconia formation.

2 Materials and methods

Ceramic slurries made of alumina and/or zircon powder, monomer, photoinitiator, and dispersant were prepared, characterized, and then a suspension of the stoichiometric mixture was used to fabricate ceramic parts by DLP additive manufacturing. These ceramic bodies were sintered at different temperatures and so characterized, as described next.

2.1 Powder preparation

Calcined Alumina powder (A1000 SG, Almatis, USA) was used as received, and commercial zircon powder (325 MESH, Minasolo, Brazil) was ground in a ball mill and subsequently in a vibrating ball mill, aiming for a powder suitable for DLP suspensions, similar to the preparation of other ceramic materials for DLP [26]. The particle size was measured by a Laser Particle Sizer (ANALYSETTE 22, Fritsch).

2.2 Slurry preparation

The slurries were composed of the ceramic powders (40 vol%), monomer (Poly(ethylene glycol) diacrylate, PEGDA M_n 250, Sigma Aldrich, USA), dispersant (DISPERBYK-111, BYK-Chemie, Germany), and photoinitiator (Phenylbis(2,4,6-trimethylbenzoyl)phosphine oxide, Sigma Aldrich, USA). The materials were mixed and then homogenized in a ball mill for 24 hours. The choice of these organic additives and this preparation protocol for photosensitive ceramic suspensions have been previously presented and discussed in previous works [26,27].

2.3 Slurry characterization

Three ceramic slurries were prepared: alumina, zircon, and alumina-zircon mixture (3:2 molar ratio). The rheological behavior of these suspensions was characterized using a rotational viscometer (DV2T extra, Brookfield, Canada) at a room temperature between 23 and 25 °C. The stability of the suspensions was investigated by sedimentation tests, in which 10 ml of each suspension was poured into graded tubes and kept undisturbed for 30 days to track sedimentation volume fraction as a function of time, as done by related works [28–30].

2.4 Additive manufacturing and post-processing

Green ceramic parts were manufactured in a bottom-up DLP 3D Printer (LD-002H, Creality) using the prepared alumina-zircon photosensitive suspensions. The layer thickness was set to 50 μm layer thickness. All the green printed parts were rinsed with isopropyl alcohol and then dried in the oven for 12 h at 100 °C. The heating rates for the debinding followed the schedule described in Table 1, which was based on a previous work [26] that used the same organic components (monomer and dispersant). The green printed parts were debound and sintered in air environment at different temperatures (1400, 1500, and 1600 °C) for 2 hours in a box furnace (Blue M, Lindberg).

Table 1: Thermal debinding schedule

Temperature (°C)	Heating hate (°C / min)	Holding time (min)
30-350	1	-
350-400	0.5	-
400-440	0.2	-
440-600	0.5	-
600	-	60

2.5 Reaction sintering and parts Characterization

The phase composition of the raw material and powder from 3D printed parts sintered at different temperatures (1400, 1500, and 1600 °C) were identified by X-ray diffraction (XDR-7000, Shimadzu). 10 wt% of Cr_2O_3 was used as the internal standard. Quantitative analysis of the diffraction patterns was performed using the Rietveld method via the X'Pert HighScore Plus v5.1 (Malvern Panalytical) software.

A Helium Gas Pycnometer (Accupyc 1330, Micromeritics) was used to measure the apparent density of the sintered parts and the true density of the powders from these parts, which were used to calculate the closed porosity. Also, the bulk density and open porosity were measured based on Archimedes' Principle using an analytical balance with a resolution of 0.01 mg (AUW220D, Shimadzu) according to ASTM-C20

Flexural three-point strength tests (span of 20 mm) were performed on ten sintered 3D printed bars with no additional machining or surface polishing (~ 25 mm x 2 mm x

1.5 mm), according to standard ASTM C1161. For this test, a universal testing machine (Bionix 370.02, MTS®) was used with a load cell of 15 kN and a crosshead speed of 0.2 mm/min.

Lastly, SEM samples were analyzed by a scanning electron microscope (SIGMA, WEISS). For this purpose, the samples were polished and thermally etched for 6 minutes at temperatures that depend on the sintering temperature, as defined by Equation 2, where T_{etch} is the etching temperature (in °C), and T_{sint} is the sintering temperature (in °C). This procedure was empirically developed by our research group and has previously shown satisfactory results for different ceramic materials such as alumina, mullite, zirconia, and hydroxyapatite.

$$T_{etch} = T_{sint} * 0.875 + 100 \quad (2)$$

3 Results and discussion

3.1 Powder characterization

Figure 1 presents the SEM images of the powders used in the ceramic suspensions. According to the analysis of the Laser Particle Sizer, the commercial alumina powder presented a mean particle size of 0.8 µm. The zircon powder reached the same mean particle size after being processed in a ball mill for 7 days and subsequently in a vibrating ball mill also for 7 days. Such value is similar to what has been used in related works [12]. Finer particles would be desirable to improve sintering reactivity [19,31,32], but they would increase the suspension viscosity, limiting the solid loading that could be added to prepare a ceramic slurry suitable for DLP additive manufacturing [19,26].

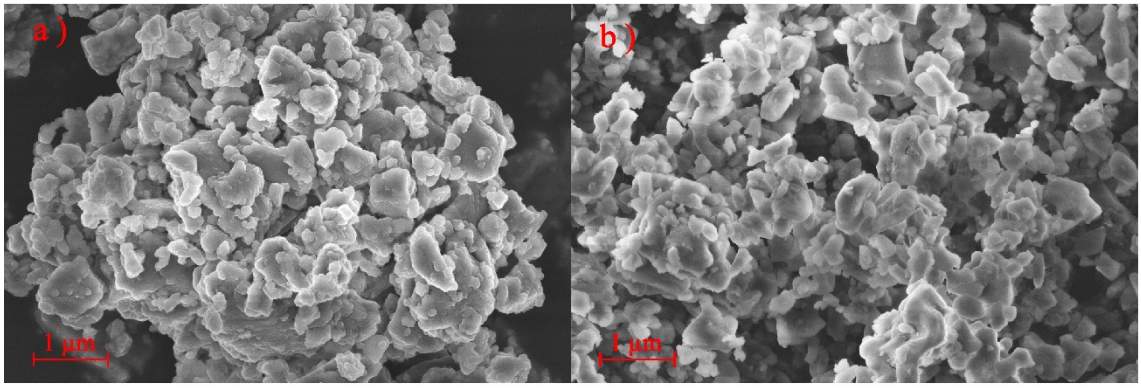

Figure 1: SEM images of the ceramic powders used in the preparation of the photosensitive suspensions. a) Calcined Alumina. b) Ground Zircon.

3.2 Slurry rheological Behavior and Stability

Figure 2 shows the viscosity curves of the prepared slurries. All the suspensions show similar viscosity in the operation range of the process (shear rate above 30 s^{-1} [19,33]), which is associated with the similar particle size of the powders. The low viscosity of the ceramic suspensions (<0.25 Pa.s) is favorable to the formation of uniform micrometric layers [28]. Also, their moderate shear-thinning behavior (decreased viscosity with increased shear rate) is desirable to avoid the sedimentation of the suspension at rest and allows adequate flow when a shear rate is applied [19,34]. Differences in the rheological behavior of suspensions may be associated with the geometry of the ceramic powders used.

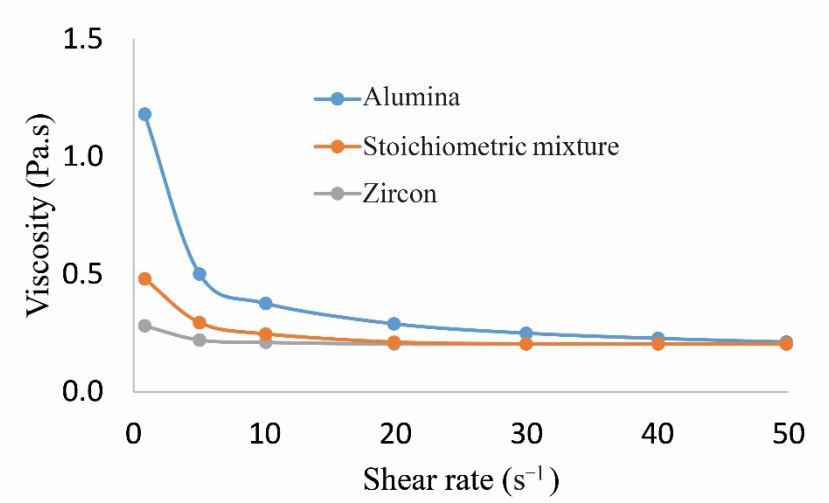

Figure 2. Viscosity curves of the prepared ceramic suspensions.

Moreover, the prepared ceramic suspensions presented negligible sedimentation during the 30 days test with the retained volume fraction greater than 95%, indicating slurries suitable for the considered AM process.

3.3 Additive manufactured parts

Figure 3 shows printed parts, indicating the ability to manufacture parts with detailed and tiny structures, which would be unfeasible or even impossible to be produced by other manufacturing processes.

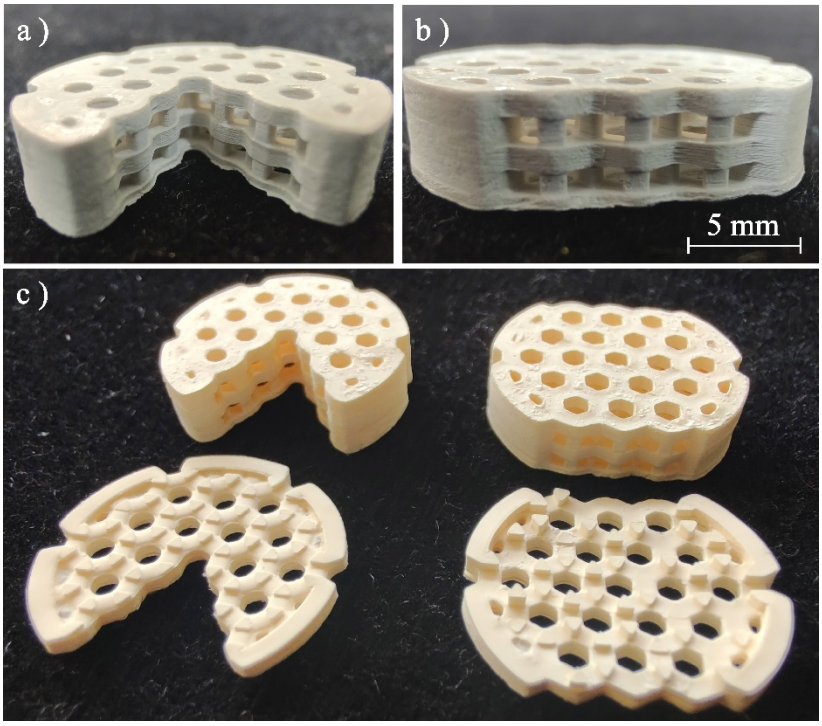

Figure 3. Printed parts with tiny structures. a) Green. b) Sintered at 1600 °C.

3.4 Reaction sintering

Figure 4 shows X-ray diffraction patterns for the initial powders and parts sintered at different temperatures. Parts sintered at 1400 °C presented the same phases as the raw materials and amorphous content of 8%. Parts sintered at 1500 °C contained not only the initial phases but also in situ mullite and monoclinic zirconia. At this temperature, zircon is dissociating, and the silica dissociated is being consumed in the formation of mullite with the alumina available in the system. At this temperature, about 5% was identified as an amorphous phase. Finally, the reaction is completed at 1600 °C, creating mullite-zirconia composites with a residual amorphous phase of 4%.

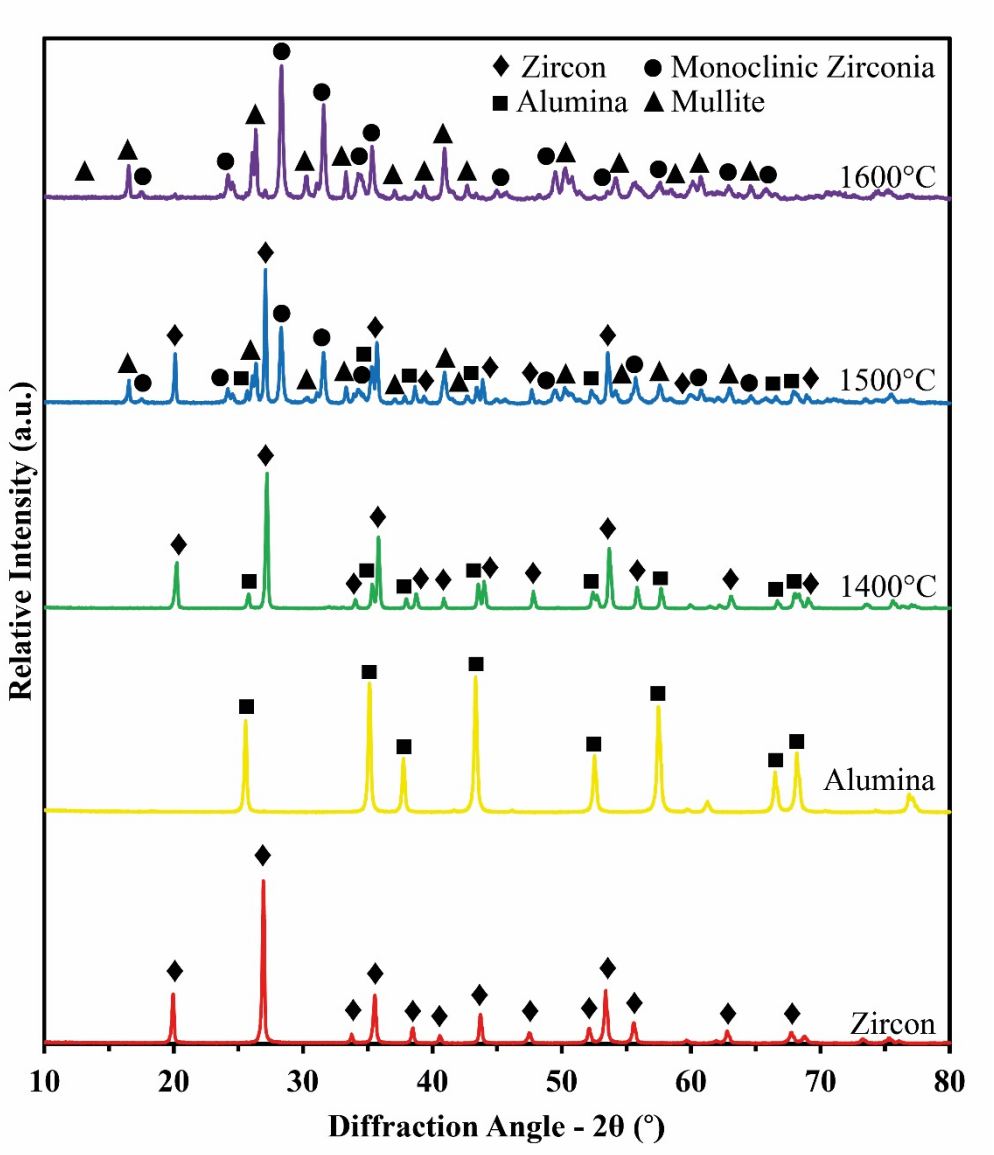

Figure 4. X-ray diffraction patterns for the initial powders and parts sintered at different temperatures.

The reaction sintering is also evidenced in the density of the powders from parts sintered at different temperatures (Figure 5). The true density of parts sintered at 1400 °C is similar to that of the initially mixed powders. The mullite and zirconia formation decreases the true density, and the powder density reached 3.740 ± 0.004 g/cm3 at 1600 °C. On the other hand, the bulk density increases with increasing sintering temperature. Thus, the relative density increased from 64 ± 1 to 88 ± 1 % when the sintering temperature increased from 1400 °C to 1600 °C. In addition, a summary of open and

closed porosity is presented in Table 2, indicating that open porosity is predominant in the 3D printed parts sintered at all temperatures studied.

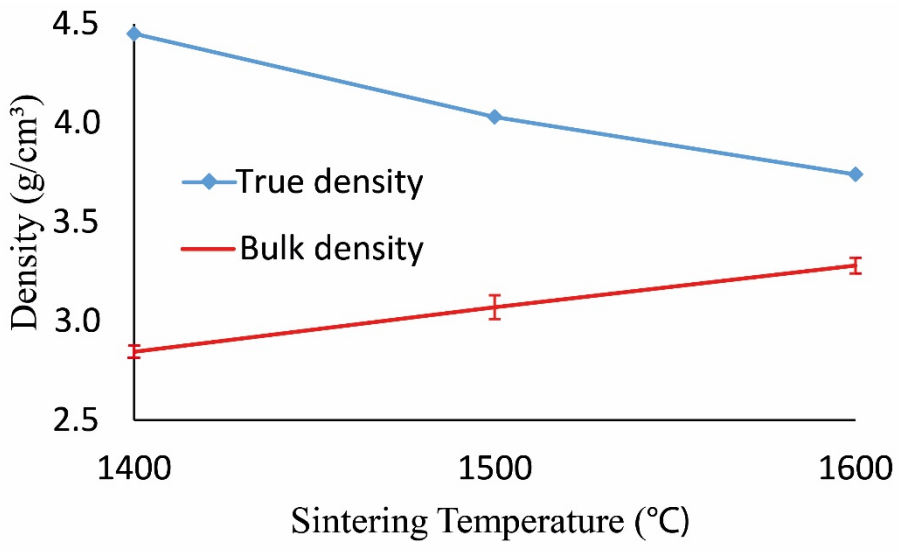

Figure 5. Influence of sintering temperature on true density and bulk density.

Table 2: Influence of sintering temperature on open and closed porosity

Sintering Temperature (°C)	Open Porosity (%)	Closed Porosity (%)
1400	31±1	4.9±0.9
1500	19±1	4.6±0.8
1600	11±1	1.4±0.5

The flexural strength of the mullite-zirconia composites after the completed reaction sintering (1600 °C) reached 84 ± 13 MPa. This value is significantly higher than the flexural strength presented by mullite parts (48 MPa) with alike relative density (86%) and manufactured under similar conditions [26]. On the other hand, research about mullite-zirconia composites produced by conventional ceramic processing has reported quite varied flexural strength. For example, Aydin and Tokatas [15] reported a remarkable improvement of the flexura strength by using a sintering additive (colemanite), and the flexural strength improved from 52-94 MPa to 106-187 MPa (depending on the solid concentration and sintering temperature). Also, Lian et al. [35] obtained up to 285 MPa of flexural strength with mullite-zirconia composites. However, such a value was

obtained for parts with open porosity smaller than 1%, being much denser than those reported in the present work.

Both relative density and flexural strength could be improved by increasing the solid loading of the suspension [34,36–39], which was limited, in this work, by the ordinary bottom-up 3D printer used. A higher ceramic loading would result in higher viscosities and demand a 3D printer specialized in ceramics [19]. Also, sintering additives have been used to improve densification in the fabrication of mullite-zirconia composites by conventional processes [15,40–43] and may be used in future developments of photosensitive suspensions to 3D print these materials.

The SEM images with element mapping of parts sintered at different temperatures are shown in Figures 6-8. Although the XRD analysis indicated a moderate fraction of amorphous in all the samples, it plays an important role in the reaction sintering. The dissociation of zircon is already happening at 1500 ºC (Figure 7), but the amorphous composition is not evident in the general EDS element mapping. However, a greater amount of impurities (Na and K) could be found in the boundaries of Zr-rich regions, as indicated in Figure 7b, suggesting the existence of a glassy phase in the area [13]. Finally, Figure 8 shows the microstructure for parts sintered at 1600 ºC, in which the formation of in situ mullite and monoclinic zirconia was completed. The rounded morphology of the monoclinic zirconia corroborates the formation of the glassy phase around Zr-rich regions during the reaction sintering, as indicated in related work [15]. The formation of monoclinic rather than tetragonal zirconia was already expected since dopants were not added in this work.

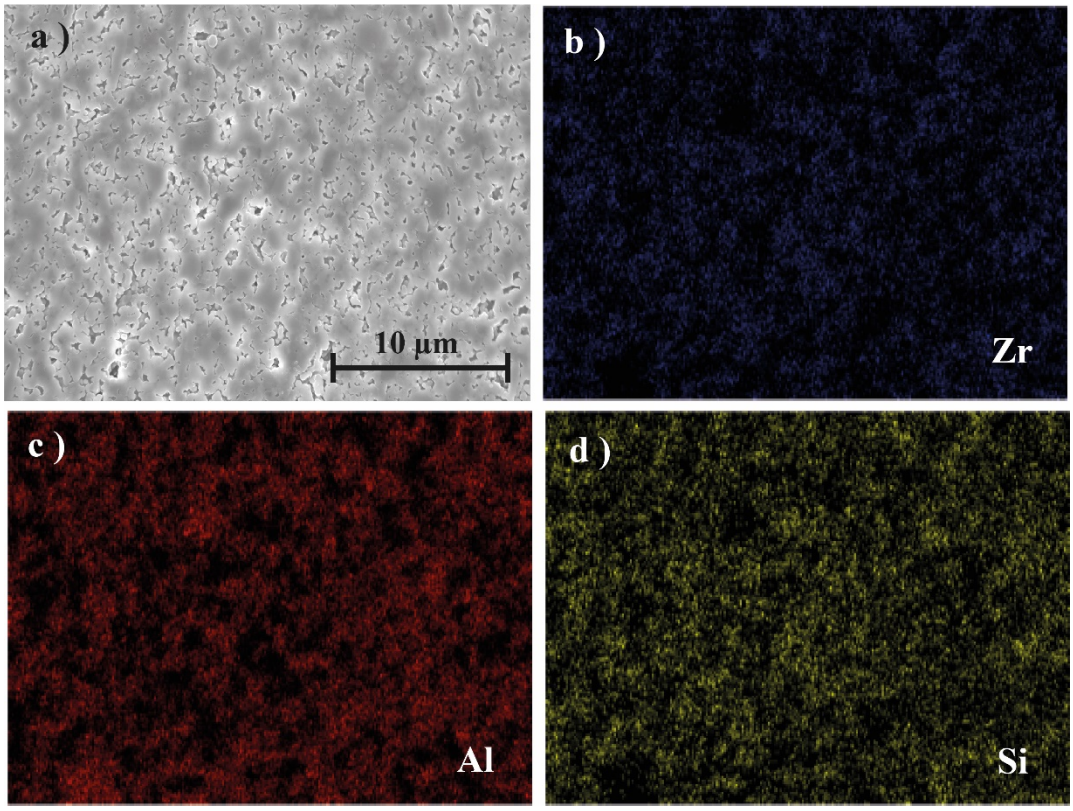

Figure 6. SEM-EDS elemental mapping of a sample sintered at 1400 °C. a) Scanning Electron Microscopy. b) Element mapping of Zr. c) Element mapping of Al. d) Element mapping of Si.

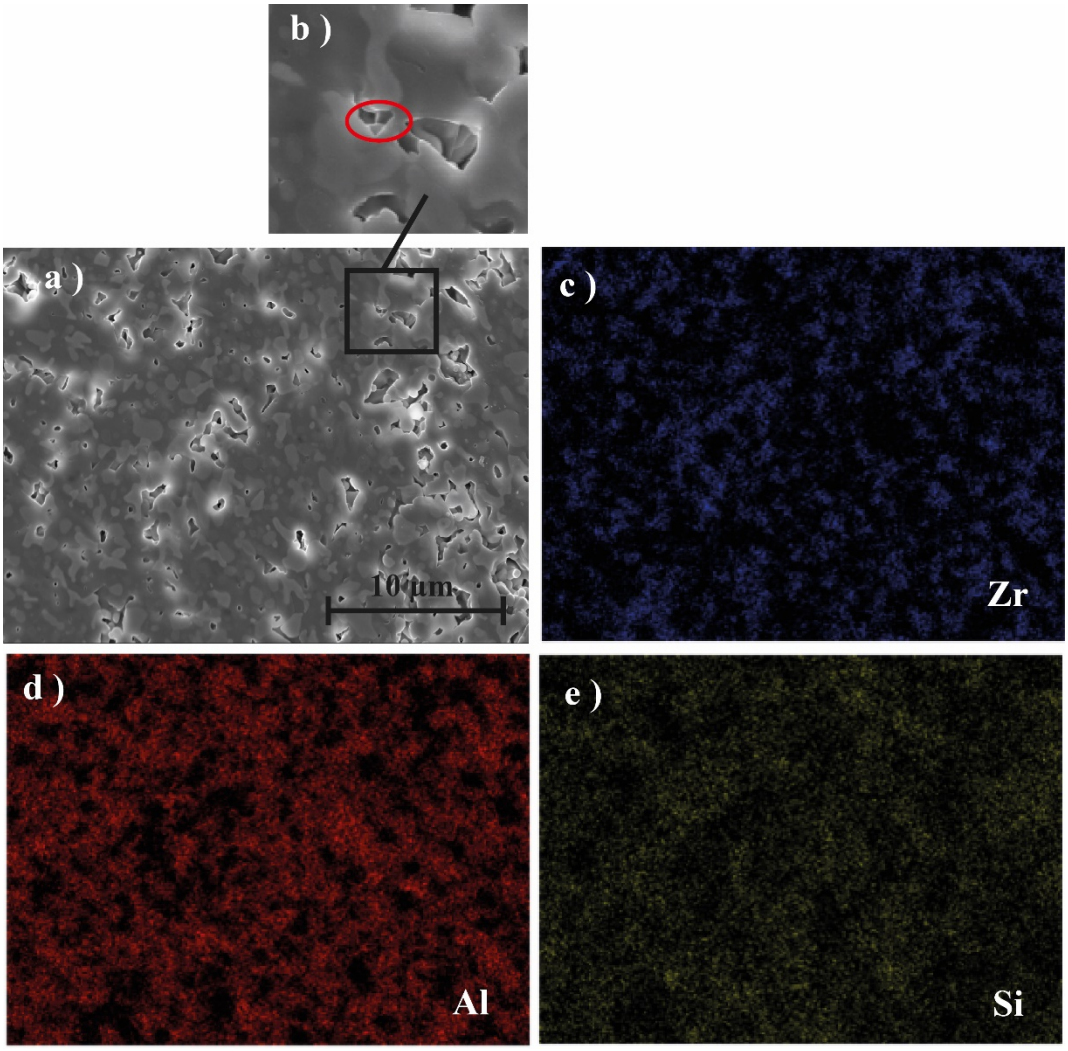

Figure 7. SEM-EDS elemental mapping of a sample sintered at 1500 °C. a) Scanning Electron Microscopy (SEM). b) Magnified view of the SEM image with an indication of an impurity-rich region. c) Element mapping of Zr. d) Element mapping of Al. e) Element mapping of Si.

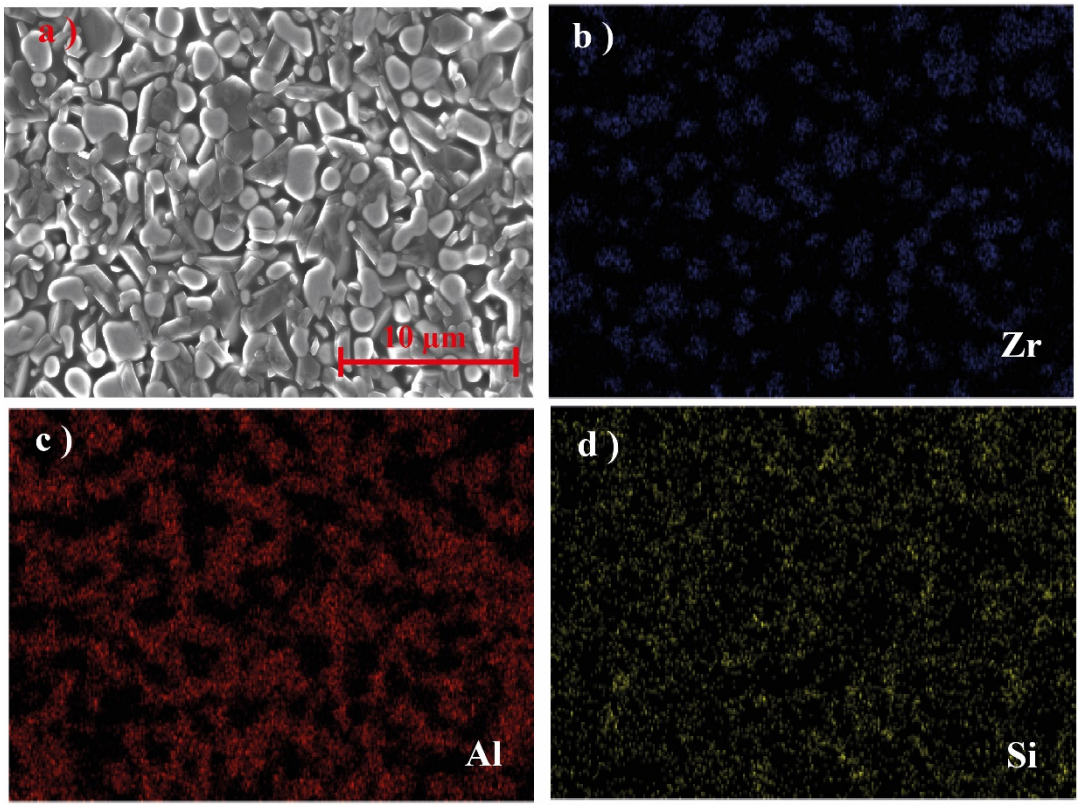

Figure 8. SEM-EDS elemental mapping of a sample sintered at 1600 °C. a) Scanning Electron Microscopy. b) Element mapping of Zr. c) Element mapping of Al. d) Element mapping of Si.

4 Conclusions

In this work, ceramic parts with tiny structures were successfully 3D printed by DLP using prepared photosensitive suspensions based on the stoichiometric mixture of alumina and ground zircon powders. Subsequently, the parts were debound and sintered at different temperatures and the formation of in situ mullite-zirconia composites was evaluated. The reaction sintering was completed at 1600 ºC, which is evidenced by the X-ray diffraction patterns, true density, and SEM images. The printed parts sintered at 1600 ºC for 2 hours reached a relative density of 87.7 ± 0.9 % and a flexural strength of 84 ± 13 MPa. Thus, a proper feedstock to additive manufacturing of mullite-zirconia composites by digital light processing was developed and the process proved to be able to manufacture detailed and tiny structures, which would be unfeasible or even impossible to be produced by other manufacturing processes.

5 Acknowledgments

This research was financially supported by Coordenação de Aperfeiçoamento de Pessoal de Nível Superior - Brasil (CAPES) - finance code 001. R.F. received support from the European Union's Horizon 2020 research and innovation programme under the Marie Skłodowska-Curie grant agreement No. 801604.

6 References

[1] R. Emadi, H. Ashrafi, R. Zamani Foroushani, Effect of temperature on the reaction sintering of mechanically activated ZrSiO4–Al2O3 mixture, Ceram. Int. 41 (2015) 14400–14405. doi:10.1016/j.ceramint.2015.07.074.

[2] R.G. Carvalho, F.J. Oliveira, R.F. Silva, F.M. Costa, Mechanical behaviour of zirconia-mullite directionally solidified eutectics, Mater. Des. 61 (2014) 211–216. doi:10.1016/j.matdes.2014.04.050.

[3] A. Khorsand, H. Majidian, M. Farvizi, Development of AMZ composites via mutual attraction of particles in wet processing, Int. J. Appl. Ceram. Technol. 17 (2020) 1822–1832. doi:10.1111/ijac.13522.

[4] A.C. Mazzei, J.A. ROdrigues, Alumina-mullite-zirconia composites obtained by reaction sintering. Part I: microstructure and mechanical behavior, J. Mater. Sci. 35 (2000) 2807–2814.

[5] S. Hazra, P.P. Bandyopadhyay, Tribological properties of plasma sprayed zircon-alumina powder mixture with and without laser re-melting, Trans. Inst. Met. Finish. 98 (2020) 144–153. doi:10.1080/00202967.2020.1757309.

[6] T. Ebadzadeh, E. Ghasemi, Influence of starting materials on the reaction sintering of mullite-ZrO2 composites, Mater. Sci. Eng. A. 283 (2000) 289–297. doi:10.1016/S0921-5093(99)00631-0.

[7] W.J. Wei, H.C. Kao, M.H. Lo, Phase Transformation and Grain Coarsening Zirconia / Mullite Composites, 2219 (1996) 239–247.

[8] L. Yuan, Z. Liu, X. Hou, Z. Liu, Q. Zhu, S. Wang, B. Ma, J. Yu, Fibrous ZrO2-mullite porous ceramics fabricated by a hydratable alumina based aqueous gel-casting process, Ceram. Int. 45 (2019) 8824–8831. doi:10.1016/j.ceramint.2019.01.209.

[9] E. Di Rupo, M.R. Anseau, Solid state reactions in the ZrO2 · SiO2 - αAl2O3 system, J. Mater. Sci. 15 (1980) 114–118. doi:10.1007/BF00552434.

[10] M.M.S. Wahsh, R.M. Khattab, M. Awaad, Thermo-mechanical properties of mullite/zirconia reinforced alumina ceramic composites, Mater. Des. 41 (2012) 31–36. doi:10.1016/j.matdes.2012.04.040.

[11] E. Medvedovski, Alumina-mullite ceramics for structural applications, Ceram. Int. 32 (2006) 369–375. doi:10.1016/j.ceramint.2005.04.001.

[12] H.M. Jang, S.M. Cho, K.T. Kim, Alumina-mullite-zirconia composites: Part 1. Colloidal processing and phase-formation characteristics, J. Mater. Sci. 31 (1996) 5083–5092. doi:10.1007/BF00355909.

[13] C. Zanelli, M. Dondi, M. Raimondo, G. Guarini, Phase composition of alumina-mullite-zirconia refractory materials, J. Eur. Ceram. Soc. 30 (2010) 29–35. doi:10.1016/j.jeurceramsoc.2009.07.016.

[14] A. Khorsand, H. Majidian, M. Farvizi, A new method for preparing AMZ composites: Coating zircon powder by aluminum alkoxide, Ceram. Int. 46 (2020) 2273–2286. doi:10.1016/j.ceramint.2019.09.216.

[15] H. Aydin, G. Tokatas, Mechanical properties of zirconia toughened mullite composites fabricated by slip casting, J. Ceram. Process. Res. 20 (2019) 250–258. doi:10.36410/jcpr.2019.20.3.250.

[16] H. Aydin, G. Tokatas, Characterization and production of slip casts mullite–zirconia composites, SN Appl. Sci. 1 (2019) 1–15. doi:10.1007/s42452-018-0061-4.

[17] M. Schwentenwein, J. Homa, Additive manufacturing of dense alumina ceramics, Int. J. Appl. Ceram. Technol. 12 (2015) 1–7. doi:10.1111/ijac.12319.

[18] K. Zhang, R. He, G. Ding, C. Feng, W. Song, D. Fang, Digital light processing of 3Y-TZP strengthened ZrO2 ceramics, Mater. Sci. Eng. A. 774 (2020) 138768. doi:10.1016/j.msea.2019.138768.

[19] I.L. de Camargo, M.M. Morais, C.A. Fortulan, M.C. Branciforti, A review on the rheological behavior and formulations of ceramic suspensions for vat photopolymerization, Ceram. Int. 47 (2021) 11906–11921. doi:10.1016/j.ceramint.2021.01.031.

[20] Y. Lakhdar, C. Tuck, J. Binner, A. Terry, R. Goodridge, Additive manufacturing of advanced ceramic materials, Prog. Mater. Sci. 116 (2021) 100736. doi:10.1016/j.pmatsci.2020.100736.

[21] J.S. Pelz, N. Ku, M.A. Meyers, L.R. Vargas-Gonzalez, Additive manufacturing of structural ceramics: a historical perspective, J. Mater. Res. Technol. 15 (2021) 670–695. doi:10.1016/j.jmrt.2021.07.155.

[22] Q. Lian, F. Yang, H. Xin, D. Li, Oxygen-controlled bottom-up mask-projection stereolithography for ceramic 3D printing, Ceram. Int. 43 (2017) 14956–14961. doi:10.1016/j.ceramint.2017.08.014.

[23] O. Santoliquido, P. Colombo, A. Ortona, Additive Manufacturing of ceramic components by Digital Light Processing: A comparison between the “bottom-up” and the “top-down” approaches, J. Eur. Ceram. Soc. 39 (2019) 2140–2148. doi:10.1016/j.jeurceramsoc.2019.01.044.

[24] M.L. Griffith, J.W. Halloran, Freeform fabrication of ceramics via stereolithography, J. Am. Ceram. Soc. 79 (1996) 2601.

[25] Z. Wu, W. Liu, H. Wu, R. Huang, R. He, Q. Jiang, Y. Chen, X. Ji, Z. Tian, S. Wu, Research into the mechanical properties, sintering mechanism and microstructure evolution of Al2O3-ZrO2 composites fabricated by a stereolithography-based 3D printing method, Mater. Chem. Phys. 207 (2018) 1–

10. doi:10.1016/j.matchemphys.2017.12.021.

[26] I.L. de Camargo, R. Erbereli, C.A. Fortulan, Additive manufacturing of electrofused mullite slurry by digital light processing, J. Eur. Ceram. Soc. 41 (2021) 7182–7188. doi:10.1016/j.jeurceramsoc.2021.07.005.

[27] I.L. de Camargo, R. Erbereli, H. Taylor, C.A. Fortulan, 3Y-TZP DLP additive manufacturing: solvent-free slurry development and characterization, Mater. Res. 24 (2021) e20200457. doi:10.1590/1980-5373-mr-2020-0457.

[28] K. Zhang, R. He, C. Xie, G. Wang, G. Ding, M. Wang, W. Song, D. Fang, Photosensitive ZrO2 suspensions for stereolithography, Ceram. Int. 45 (2019) 12189–12195. doi:10.1016/j.ceramint.2019.03.123.

[29] Z. Chen, J. Li, C. Liu, Y. Liu, J. Zhu, C. Lao, Preparation of high solid loading and low viscosity ceramic slurries for photopolymerization-based 3D printing, Ceram. Int. 45 (2019) 11549–11557. doi:10.1016/j.ceramint.2019.03.024.

[30] K. Zhang, C. Xie, G. Wang, R. He, G. Ding, M. Wang, D. Dai, D. Fang, High solid loading, low viscosity photosensitive Al2O3 slurry for stereolithography based additive manufacturing, Ceram. Int. 45 (2019) 203–208. doi:10.1016/j.ceramint.2018.09.152.

[31] Z. Wang, C. Huang, J. Wang, B. Zou, Development of a novel aqueous hydroxyapatite suspension for stereolithography applied to bone tissue engineering, Ceram. Int. 45 (2019) 3902–3909. doi:10.1016/j.ceramint.2018.11.063.

[32] Diptanshu, G. Miao, C. Ma, Vat photopolymerization 3D printing of ceramics: Effects of fine powder, Manuf. Lett. 21 (2019) 20–23. doi:10.1016/j.mfglet.2019.07.001.

[33] X. Li, H. Zhong, J. Zhang, Y. Duan, H. Bai, J. Li, D. Jiang, Dispersion and properties of zirconia suspensions for stereolithography, Int. J. Appl. Ceram. Technol. 17 (2020) 239–247. doi:10.1111/ijac.13321.

[34] M. Borlaf, A. Serra-Capdevila, C. Colominas, T. Graule, Development of UV-curable ZrO2 slurries for additive manufacturing (LCM-DLP) technology, J. Eur. Ceram. Soc. 39 (2019) 3797–3803. doi:10.1016/j.jeurceramsoc.2019.05.023.

[35] W. Lian, Z. Liu, R. Zhu, W. Wang, Y. Liu, S. Wang, Y. Wang, Y. Liu, L. Kong, Effects of zirconium source and content on zirconia crystal form, microstructure and mechanical properties of ZTM ceramics, Ceram. Int. 47 (2021) 19914–19922. doi:10.1016/j.ceramint.2021.03.327.

[36] K. Zhang, Q. Meng, X. Zhang, Z. Qu, S. Jing, R. He, Roles of solid loading in stereolithography additive manufacturing of ZrO2 ceramic, Int. J. Refract. Met. Hard Mater. 99 (2021) 105604. doi:10.1016/j.ijrmhm.2021.105604.

[37] W. Liu, M. Li, J. Nie, C. Wang, W. Li, Z. Xing, Synergy of solid loading and printability of ceramic paste for optimized properties of alumina via stereolithography-based 3D printing, J. Mater. Res. Technol. 9 (2020) 11476–11483. doi:10.1016/j.jmrt.2020.08.038.

[38] M. Borlaf, N. Szubra, A. Serra-Capdevila, W.W. Kubiak, T. Graule, Fabrication of ZrO2 and ATZ materials via UV-LCM-DLP additive manufacturing

technology, J. Eur. Ceram. Soc. 40 (2020) 1574–1581. doi:10.1016/j.jeurceramsoc.2019.11.037.

[39] H. Xing, B. Zou, S. Li, X. Fu, Study on surface quality, precision and mechanical properties of 3D printed ZrO2 ceramic components by laser scanning stereolithography, Ceram. Int. 43 (2017) 16340–16347. doi:10.1016/j.ceramint.2017.09.007.

[40] H. Aydın, Effect of La2O3 addition on the thermal, microstructure and mechanical properties of mullite–zirconia composites, Iran. J. Mater. Sci. Eng. 16 (2019) 10–19. doi:10.22068/ijmse.16.4.10.

[41] D. Chandra, G. Das, S. Maitra, Comparison of the Role of MgO and CaO Additives on the Microstructures of Reaction-Sintered Zirconia-Mullite Composite, Int. J. Appl. Ceram. Technol. 12 (2015) 771–782. doi:10.1111/ijac.12263.

[42] S. Bodhak, S. Bose, A. Bandyopadhyay, Densification Study and Mechanical Properties of Microwave-Sintered Mullite and Mullite-Zirconia Composites, J. Am. Ceram. Soc. 94 (2011) 32–41. doi:10.1111/j.1551-2916.2010.04062.x.

[43] D.H.A. Besisa, E.M.M. Ewais, Investigation of mechanical strength of the functionally graded zirconia-mullite/alumina ceramics tailored for high temperature applications, Mater. Res. Express. 6 (2019). doi:10.1088/2053-1591/ab177e.